Food Chemistry: X 20 (2023) 100990

Contents lists available at ScienceDirect

Food Chemistry: X

journal homepage: www.sciencedirect.com/journal/food-chemistry-x

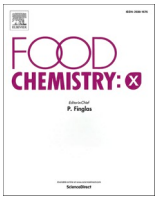

# A novel photothermal sensing probe based on violet phosphorus for sensitive immunochromatographic sensing detection

Zhen Zhang [a,1], Zhenkai Hao [a,1], Ruiping Shan [a], Muhammad Wasim Tasleem [a], Jianbin Wang [b], Jianhua Zhou [a,*], Hongyan Zhang [a,*]

[a] Shandong Provincial Key Laboratory of Animal Resistance Biology, Key Laboratory of Food Nutrition and Safety of Shandong Normal University, College of Life Sciences, Shandong Normal University, Jinan 250014, PR China
[b] Zhucheng Dongxiao Biotechnology Co., Ltd., Weifang, 262200, PR China

ARTICLE INFO

*Keywords:*
Violet phosphorus
Photothermal sensing
Immunochromatographic
Diethylstilbestrol

ABSTRACT

Photothermal immunochromatographic sensor is an emerging detection technology, and it is important to develop new sensing probes with excellent photothermal performance to improve its detection performance. In the present study, a novel photothermal sensing probe based on violet phosphorus nanosheets with satisfactory photothermal conversion efficiency (31.1 %) was reported for the first time. A photothermal immunochromatographic sensor using the above probe was applied for visual and photothermal detection of diethylstilbestrol. The diethylstilbestrol concentration was inversely proportional to photothermal sensing signal and showed a good linear correlation in the range of 0.75 ~ 50 μg·L$^{-1}$. After optimizing, the visual and photothermal detection limits were 6 μg·L$^{-1}$ and 0.56 μg·L$^{-1}$, respectively. The recovery rates in tap water, milk and pork samples ranged from 82.2 % to 115.2 %, with a coefficient of variation (CV) ranging from 2.0 % to 10.8 %. This work not only structured a new type of photothermal probe, but also expanded the application range of violet phosphorus.

## 1. Introduction

In recent years, immunochromatographic sensors have been widely used in the field of COVID-19 detection, food safety and environmental pollution monitoring due to their advantages of simple operation, short detection time and point-of-care testing (Li, Li, Wang, Liu, Zhang, Li, et al., 2023; Yuan, Chen, Wan, Li, & Liu, 2022). The test results of conventional immunochromatographic sensors based on colloidal gold nanoparticles were usually determined by visual inspection, which was easy to cause false positive or negative results and can not achieve quantitative detection (Ji, Huang, Cheng, Hao, Liu, Liu, et al., 2023; Younes, Yassine, Kourentzi, Tang, Litvinov, Willson, et al., 2023). To reduce the false positive or negative rate, several strategies have been developed. For example, enzymes or nano-enzymes have been used as signal amplifying materials to enhance the intensity of color signals, but their practical applications were limited by enzyme inactivation and complex choices of reaction substrates (Liu, Zhan, Qin, Sackrison, & Bischof, 2021; Xiao, Hu, Lai, Peng, & Lai, 2021). In order to achieve quantitative detection, a series of new labeling materials with fluorescence (Zhang, Zhang, Lai, Su, He, Lai, et al., 2023), magnetic (Salvador, Gallo Cordova, Moyano, Martínez García, Blanco López, Puerto Morales, et al., 2020), or Raman (Tu, Wu, Yu, Li, Zheng, Qi, et al., 2023) signals have been synthesized. However, the results of immunochromatographic sensors based on the aforementioned materials were susceptible to spontaneous signals and high background noise (Lu, Liu, Cai, Zhao, Cui, Zhang, et al., 2022). Additionally, expensive and complex signal acquisition instruments further limited their practical application (Ji et al., 2023).

In recent years, photothermal immunochromatographic sensing for detection has become a research hotspot because of its low cost, convenient operation and low background signal (Wang, Wang, Wang, Hao, Han, Wang, et al., 2023; Wei, Rao, Niu, Xue, Luo, Zhang, et al., 2021). Photothermal sensing probes can generate temperature variations under laser irradiation that scale linearly with the target concentration, enabling quantitative detection of hazardous substances (Wang et al., 2023). The raw material of the photothermal probe is the core of the above method. Recently, a variety of photothermal materials have been developed as sensing probes to prepare photothermal

* Corresponding authors.
*E-mail addresses:* zhoujh16@sdnu.edu.cn (J. Zhou), zhanghongyan@sdnu.edu.cn (H. Zhang).
[1] Contributed equally to the work.

https://doi.org/10.1016/j.fochx.2023.100990
Received 17 August 2023; Received in revised form 27 October 2023; Accepted 8 November 2023
Available online 11 November 2023

immunochromatographic sensors. For example, Zhang et al. (Zhang, Lei, Tian, Ren, Lu, Liu, et al., 2021) developed a $Fe_3O_4$@Au photothermal sensing probe and successfully constructed a competitive immunochromatographic sensor for micromolecule detection. Liang et al. (Liang, Cai, Gao, Yan, Fu, Tang, et al., 2022) synthesized a polydopamine-Cu photothermal sensing probe and used it to construct a double-antibody sandwich immunochromatographic sensor capable of detecting macromolecules. As research has deepened, it has been shown that raw materials with higher photothermal conversion efficiency can effectively improve the detection sensitivity (Shang, Zhang, Ding, Zhang, & Wang, 2023; Zhang, Huang, Ren, Chen, Yan, Dai, et al., 2023). Therefore, the development of new raw materials with better performance is a focus of research in the field of photothermal detection.

As a novel photothermal material, phosphorus-based nanosheets have attracted much attention due to their excellent photothermal performance, which benefit from the adjustable band gap (Ren, Philo, Li, Shi, Chang, & Ye, 2020). Phosphorus nanosheets have a variety of allotropes, of which black phosphorus is a typical representative. Black phosphorus has been widely used in the field of photothermal therapy (Hou, Fei, Liu, Liu, Li, & Luo, 2022). However, it is extremely unstable in water and oxygen, limiting its further application (Zhao, Wang, Huang, Xiao, Xu, Guo, et al., 2016). Violet phosphorus was reported in the 1860 s as an allotrope of black phosphorus with advantages such as better stability, wider tunable band gap, and higher carrier mobility than black phosphorus (Zhang, Huang, Zhang, Gu, Zhao, Zhao, et al., 2020). Most of the previous studies have focused on how to efficiently prepare violet phosphorus and explored its photoelectric, photocatalytic, fluorescence properties. For instance, Zhang et al. (Zhang, Gu, Li, Zhao, Fu, Liu, et al., 2020) reported on the method for obtaining high crystallinity violet phosphorus with a high yield. Zhou et al. (Zhou, Kang, Dong, Wang, Li, Huang, et al., 2023) investigated the application performance of violet phosphorus in the field of ultrafast nonlinear optical devices. Wang et al. (Wang, Zhao, Liu, Yang, Pang, Gao, et al., 2023) explored the photocatalytic degradation capability of violet phosphorescence. Zhao et al. (Zhao, Liu, Zhao, Gu, Zhang, Jin, et al., 2022) reported the fluorescence properties of quantum dots based on violet phosphorus. However, few studies have explored the photothermal properties and applications of violet phosphorus.

In this paper, violet phosphorus nanosheets were prepared by ultrasonic spalling method. The photothermal properties and stability of violet phosphorus nanosheets were investigated systematically. A photothermal sensing probe was prepared by coupling violet phosphorus nanosheets with anti-diethylstilbestrol monoclonal antibodies through electrostatic adsorption. Subsequently, an immunochromatographic method for the detection of diethylstilbestrol was established based on the photothermal effect of violet phosphorescence, and a quantitative analysis of compound was achieved. To the best of our knowledge, violet phosphorene has not been reported as a photothermal material for use in immunochromatographic methods. Therefore, the photothermal sensing probe based on violet phosphorus proposed in this paper can be used as a new type of photothermal probe to meet the need of improving the detection sensitivity of immunochromatographic sensors, and further expand the application range of violet phosphorus.

## 2. Material and methods

### 2.1. Materials and instruments

Violet phosphorus crystalline powder was provided by Beike Nano Technology Co., Ltd. (Suzhou, China, >99.998 %). Diethylstilbestrol (PubChem CID: 448537), hexoestrolum (PubChem CID: 3606) and bovine serum albumin (BSA, PubChem SID: 56312734) were provided by Yuanye Biological Technology Co., Ltd. (Shanghai, China, >98 %). Diethylstilbestrol monoclonal antibody, antigen and goat anti-mouse IgG were provided by Shenzhen Anti Biotechnology Co., Ltd. (Shenzhen, China). 17α-estradiol (PubChem CID: 68570), 17β-estradiol (PubChem CID:68570), estriol (PubChem CID: 5756), estrone (PubChem CID: 5870), bisphenol A (PubChem CID: 6623), bishydroxyphenylbutane (PubChem SID: 254784624) were provided by Shanghai Ruiyong Biotechnology Co., Ltd. (Shanghai, China, >98 %). Tween-20 (PubChem CID: 443314) was provided by Tianjin Huateyan Science and Technology Co., Ltd. (Tianjin, China, analytical pure). Skimmed milk powder was provided by Shanghai Epizyme Biomedical Technology Co., Ltd. (Shanghai, China). Nitrocellulose membrane was provided by Pall India Pvt Co., Ltd. (VIVI9025100R, Maharashtra, India). Sample pad (Fusion3), polyvinyl chloride sheets (DB-6) and absorption pad (H5072) was provided by Shanghai Jieyi Biotechnology Co., Ltd. (Shanghai, China). Methanol was provided by Sinopharm Group Co., Ltd. (Shanghai, China, analytical pure). Acetonitrile (PubChem CID: 6342) was provided by Shanghai Macklin Biochemical Technology Co., Ltd. (Shanghai, China, chromatographically pure). Ultrapure water (18.2 MΩ) was used for all of the experiments.

The thermal imager and 808 nm laser were used for thermal signals collection and irradiation, which provided by FOTRIC Technology Co., Ltd. (225, Shanghai, China) and Xilong Photoelectric Technology Co., Ltd. (ADR-1860, Shanghai, China), respectively. Ultrasonic cleaner and ultrasonic cell crusher were used for the synthesis of violet phosphorus nanosheets and provided by Kunshan Ultrasonic Instrument Co., Ltd. (KQ-250DE, Suzhou, China) and Sonics & Materials Co., Ltd. (VCX500, Connecticut, America), respectively. The microstructure and crystal information of violet phosphorus nanosheets was characterized by transmission electron microscope (TEM, TM3030, Tokyo, Japan) and X-ray diffraction (XRD, D8 ADVANCE, Bruker, Germany), respectively. The particle size was measured by dynamic light scattering (ZEN3600, Britain). The chemical composition was characterized by X-ray photoelectron spectroscopy (XPS, 250Xi, Massachusetts, USA). The Raman characteristic peaks of violet phosphorus were obtained by Raman microscope (HORIBA JY, Japan). The detection results of high performance liquid chromatography (HPLC) were obtained by Waters e2695100-240 V (Massachusetts, USA).

### 2.2. Synthesis of violet phosphorus nanosheets

Twenty milligrams of violet phosphorus crystal powder were weighed, placed in an agate mortar, and 2 mL of methanol was added. The powder was fully ground for 40 min to make it uniform, and then dried in the oven. The ground powder was dispersed in 60 mL of ultrapure water and subjected to 250 W ultrasound for 15 min to ensure complete dispersion in the ultra-pure water. Subsequently, it was treated with 500 W ultrasound for 6 h. After the aforementioned treatment, the supernatant was centrifuged at 514 rcf for 5 min to obtain a violet phosphorus nanosheets solution, which was then stored at 4 ℃ for future use (Zhang, Li, Qiao, Hu, Gu, Deng, et al., 2021).

### 2.3. Investigation of the photothermal properties and stability of violet phosphorus nanosheets

The photothermal properties of violet phosphorus nanosheets were measured by thermal imager and 808 nm laser (0.4 $W{\cdot}cm^{-2}$). The temperature changes of different concentrations of violet phosphorus nanosheets solution were tested. The photothermal conversion efficiency was further measured as the previous report (Lu et al., 2022). The violet phosphorus nanosheets were dispersed into PBS and oscillated in the air for 7 days. The stability of the nanosheets was investigated by measuring the temperature rise and the ratio of the absorbance value.

### 2.4. Preparation of photothermal sensing probe based on violet phosphorus

The violet phosphorus nanosheet solution was diluted until the absorbance was 1.0 at 450 nm (0.25 $mg{\cdot}mL^{-1}$). The pH of the nanosheet solution was adjusted to 8.0 by adding a potassium carbonate solution

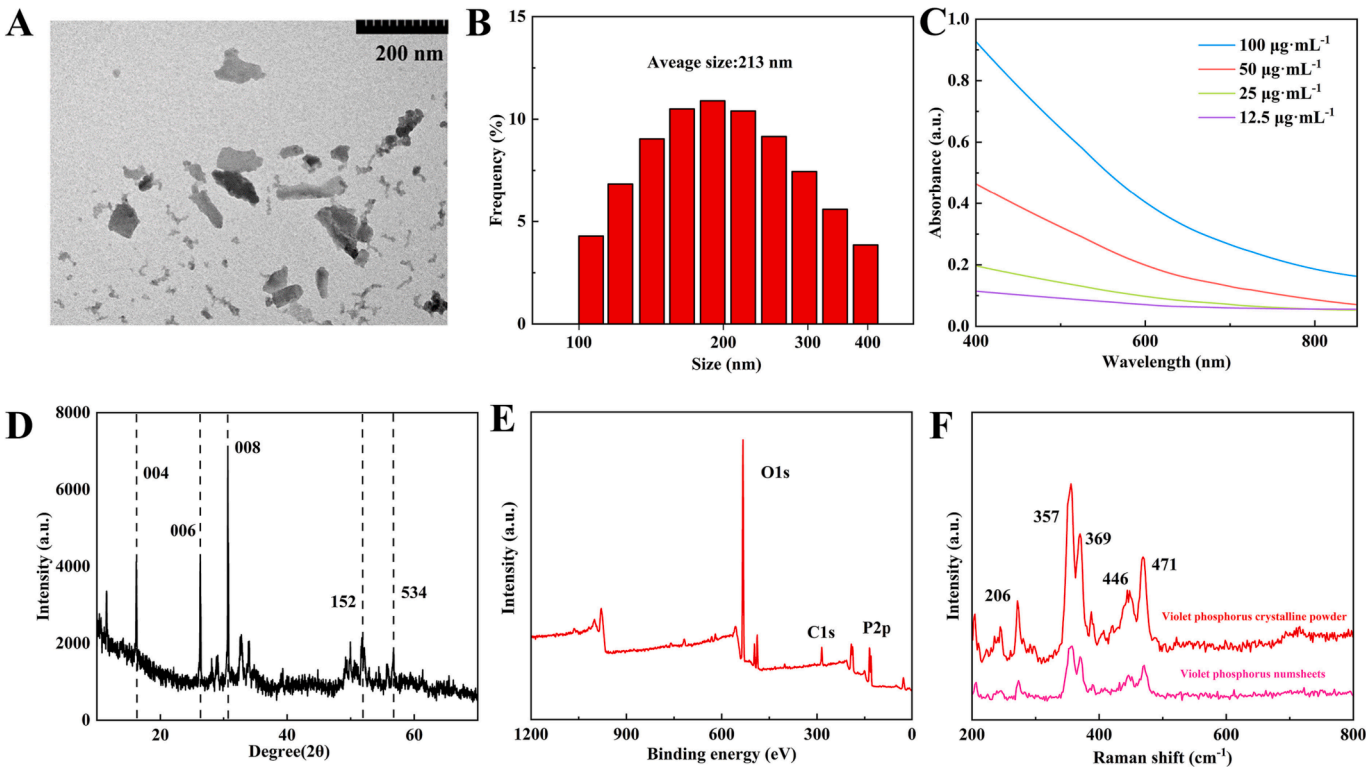


**Fig. 1.** TEM image (A), size distribution (B), ultraviolet absorption spectrum (C), XRD pattern (D), XPS spectra (E) and Raman spectra (F) of violet phosphorus nanosheets.

(0.1 mol·L$^{-1}$). Then, 400 μL of the above solution was placed in the oscillator for 5 min. The anti-diethylstilbestrol antibody was diluted to 1 mg·mL$^{-1}$ with 0.01 mol·L$^{-1}$ phosphate buffered saline (PBS), and 1.6 μL of the antibody was added to the prepared violet phosphorus nanosheets solution. It was then shaken at 37℃ for 45 min. After the shock operation, 40 μL of 10 % skimmed milk powder and 40 μL of 10 % PEG-20000 were added to the solution and blocked at 4℃ for 30 min. Then, the solution was centrifuged at 18,514 rcf (4 ℃) for 20 min. After removing the supernatant, the precipitate was suspended in 80 μL probe storage solution and stored at 4 ℃ for later use (Wang, Wang, Li, & Zhang, 2023).

### 2.5. Construction of immunochromatography sensor

The immunochromatography sensor was constructed by sample pad, nitrocellulose membrane, polyvinyl chloride sheets and absorption pad. Antigen and goat anti-mouse IgG were sprayed at a rate of 1 μL·cm$^{-1}$ in the detection and control areas, respectively. The pH of violet phosphorus nanosheets conjugated to antibody was optimized from 6.0 to12.0. The optimal range for blocking buffer consisted of skim milk powder and Tween-20 was 0.5 % ~ 2 %. The concentrations of diethylstilbestrol monoclonal antibody were optimized from 0 to 10 μg·mL$^{-1}$. The concentrations of antigen and secondary were optimized from 0.5 to 0.8 mg·mL$^{-1}$ and 0.2 to 0.5 mg·mL$^{-1}$, respectively. The amount of photothermal sensing probes was optimized from 5 to 25 μL. The laser irradiation power and time were optimized from 0.75 to 1.5 W and 0 to 75 s, respectively.

### 2.6. Diethylstilbestrol detection procedure

The sensing probes based on violet phosphorus nanosheets were added to the sample solution containing diethylstilbestrol, and then the running buffer was added. The running buffer was prepared as follows: 1 g sucrose and 800 mg BSA were dissolved in 10 mL ultrapure water, then 100 μL Tween-20 was added in the above solution. After incubating for 3 ~ 5 min, the above solution was loaded into the sample pad of the immunochromatographic sensor. Ten minutes later, visual detection results were obtained. To achieve quantitative detection, the control and test areas were irradiated with 808 nm laser, respectively. The standard curve was established by using the temperature difference between control and test areas (ΔT) and concentration of diethylstilbestrol. The detection range, sensitivity and storage stability of the immunochromatographic sensor were investigated. The addition and recovery experiments of diethylstilbestrol in tap water, milk and pork were performed in the concentration range of 7.5 to 30 μg·L$^{-1}$.

The detection conditions of HPLC were as follows, the column was C18 with the size of 250 mm × 4.6 mm (5 μm). The mobile phase was acetonitrile and water with a volume ratio of 1:1. The column temperature, flow rate, injection volume and detection wavelength was 25 °C, 1.0 mL·min$^{-1}$, 20.0 μL, and 205 nm, respectively (Xia, Hu, Liu, Zhao, & Zeng, 2022).

## 3. Results and discussion

### 3.1. Characterization of violet phosphorus nanosheets

The violet phosphorus nanosheets were obtained by ultrasonic stripping and their microstructure was characterized by TEM. As shown in Fig. 1A, violet phosphorus nanosheets exhibited lamellar structure and good dispersion, with a particle size of approximately 200 nm. The size distribution of the violet phosphorus nanosheets was further measured by nanoparticle size analyzer. The results showed that the particle size ranged from 100 nm to 400 nm, with an average particle size of about 213 nm (Fig. 1B).

Fig. 1C showed the ultraviolet absorption spectrum of violet phosphorus nanosheets. The prepared nanosheets displayed a broad absorption in the range of 400 ~ 850 nm with no impurity peaks, and the absorbance value increased significantly with increasing nanosheets

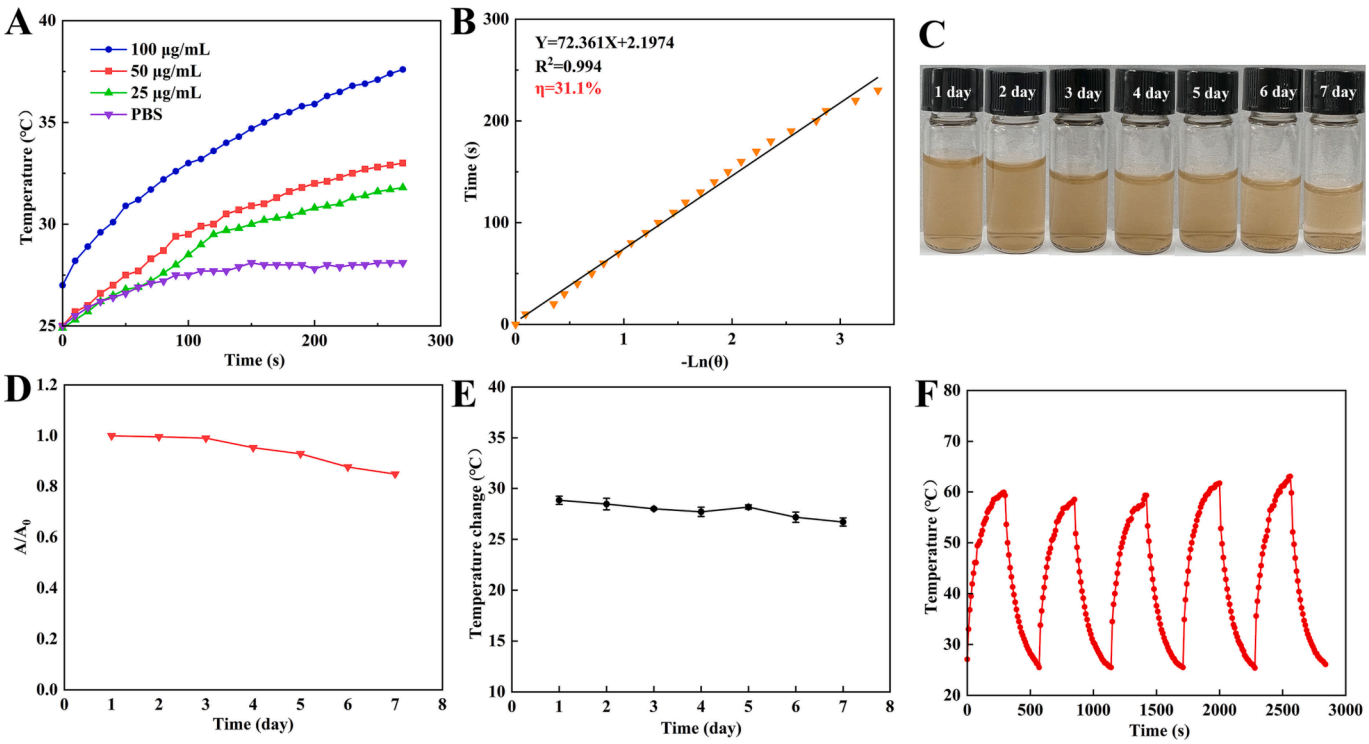


**Fig. 2.** (A) Temperature changes of PBS and violet phosphorus nanosheets solution with different concentrations. (B) The photothermal conversion efficiency of violet phosphorus nanosheets. (C) Photographs of violet phosphorus nanosheets after storing in PBS for 7 days. (D) The ratio of the absorbance value measured each day (A) to the absorbance value measured on the first day ($A_0$) during the 7-day test. (E) Temperature change of violet phosphorus nanosheets during storage in PBS for 7 days. (F) Experiment involving five photothermal cycles of violet phosphorus nanosheets.

concentration. The wide absorption spectrum is conducive to the light absorption of the material, indicating that the violet phosphorus nanosheets have a good potential for photothermal conversion. From the XRD results, it was observed that the diffraction peaks at 16.21°, 26.35°, 30.67°, 52.15° and 56.8° were correspond to (004), (006), (008), (152) and (534) crystal surfaces in violet phosphorus crystal, respectively as shown in Fig. 1D (Jin, Wang, Gu, Zhao, Zhao, Zhang, et al., 2023). The X-ray photoelectron spectroscopy (XPS) results showed $O_{1s}$, $C_{1s}$ and $P_{2p}$ peaks, which indicated that the violet phosphorus nanosheets were mainly composed of phosphorus and little oxidation (Fig. 1E) (Zhang et al., 2021). The Raman spectra of violet phosphorus nanosheets and violet phosphorus crystalline powder were measured, respectively. The Raman characteristic peaks of violet phosphorus were found at 206, 357, 369, 446 and 471, which were consistent with the previous literature (Fig. 1F) (Wang, Ma, Zhao, Jiang, Wang, Wang, et al., 2023).

### 3.2. *Photothermal properties and stability of violet phosphorus nanosheets*

To investigate the photothermal properties of the violet phosphorus nanosheets, an 808 nm laser with a power of 0.4 W $cm^{-2}$ was used to irradiate a series of violet phosphorus nanosheets solution with varying concentrations. The temperature changes were recorded in real time, accordingly. Compared to PBS, the temperature of violet phosphorus nanosheets solution was significantly higher and proportional to its concentration (Fig. 2A). The photothermal conversion efficiency was further measured. As shown in Fig. S1, the violet phosphorus nanosheets solution was irradiated by 808 nm laser until the temperature stopped rising. The laser was then turned off, and the temperature change during the cooling process was recorded. After calculation, the photothermal conversion efficiency of violet phosphorus nanosheet was 31.1 % (Fig. 2B), which was higher than that of black phosphorus (27.7 %) (Zhang et al., 2021). In addition, the photothermal property of violet phosphorus nanosheet was also better than those of conventional photothermal materials based on Au (Zhou, Huang, Zhao, Guo, Cui, Li, et al., 2022), Cu (Huang, Lin, Li, Rong, Wang, Wang, et al., 2013), and Pt (Chen, Kuo, Lee, Hwu, Chou, Chen, et al., 2013) (Table S1).

In order to assess the stability, the prepared nanosheets were dispersed into PBS and subjected them to oscillation in the air for 7 days. During the entire experiment, the color of the solution did not change significantly, and no obvious aggregation occurred (Fig. 2C). In previous reports, black phosphorus has degraded and the color of the solution changed from black to colorless after seven days of exposure to air in PBS. The ultraviolet absorption spectra of the violet phosphorus nanosheets were measured once a day and showed no remarkable changes (Fig. S2). Besides, the ratio of the absorbance value measured each day (A) to the absorbance value measured on the first day ($A_0$) was further calculated, the results were shown in Fig. 2D. No significant decrease was observed during the 7-day test, indicating that violet phosphorus nanosheets had good stability in PBS. Furthermore, the photothermal properties of the violet phosphorus were also investigated. As shown in Fig. 2E, the temperature change generated by the laser irradiation was relatively constant during the whole test period. Previous studies have shown that the photothermal properties of black phosphorus almost completely disappeared after 7 days of air exposure in PBS, which further proved that violet phosphorus had good stability (Zhang et al., 2021). Additionally, five photothermal cycle experiments were carried out on violet phosphorus nanosheets (Fig. 2F). The temperature changes in the experimentation were similar, also indicating that the violet phosphorus nanosheets had good photothermal stability.

Based on the above results regarding photothermal properties and stability, it is demonstrated that violet phosphorus is promising to be developed as a novel photothermal sensing probe for applications in photothermal detection.

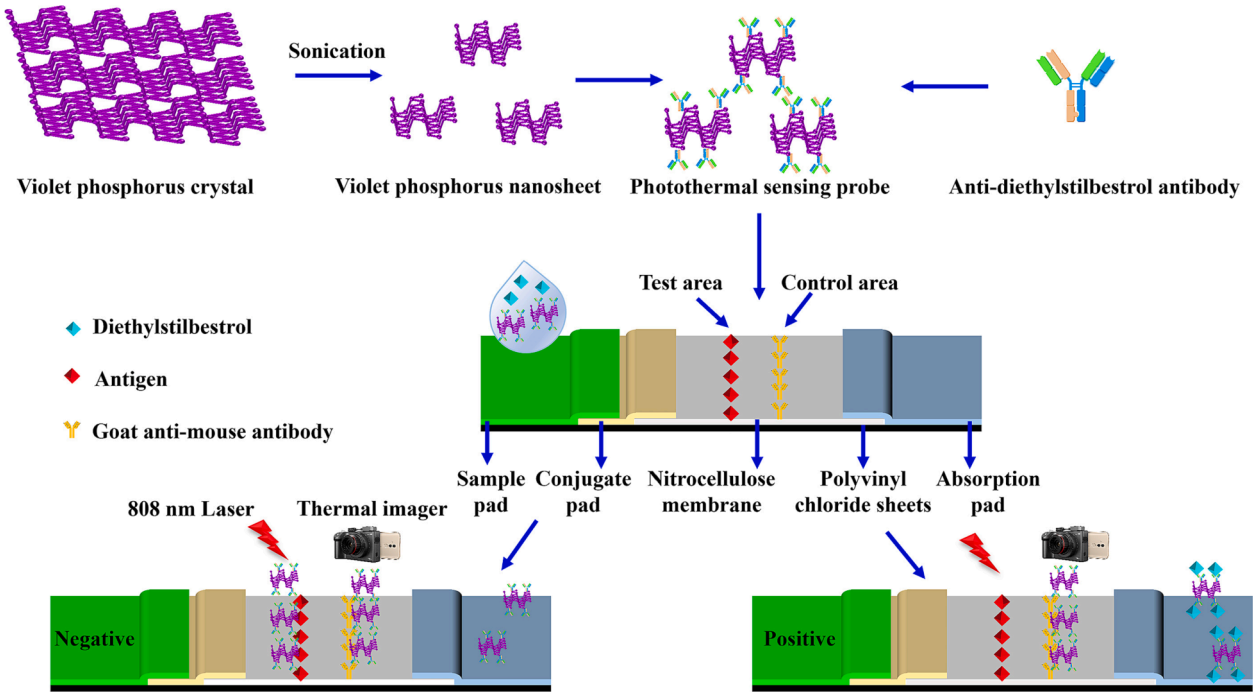


**Scheme 1.** The principle of the immunochromatographic sensing detection method based on violet phosphorus.

### *3.3. Establishment of immunochromatography sensor based on violet phosphorus nanosheet*

The principle of the proposed immunochromatographic detection method was shown in Scheme 1. Firstly, violet phosphorus nanosheets were prepared by ultrasound and coupled with anti-diethylstilbestrol antibody through electrostatic adsorption to prepare photothermal sensing probes. Subsequently, antigens and secondary antibodies were sprayed onto immunochromatographic sensors to form test and control areas. Finally, the samples were incubated with the prepared photothermal sensing probes and loaded onto the immunochromatographic sensors. An 808 nm laser was used to irradiate the test and control areas, and the temperature changes in each area were recorded. The standard curve relating the temperature differences to the diethylstilbestrol concentration was constructed for quantitative analysis.

To obtain the best test results, we conducted a comprehensive investigation to analyze the pH of violet phosphorus nanosheets conjugated with antibody, the blocking buffer, the ratio of violet phosphorus nanosheets to antibody, the concentration of antigen and secondary antibody. Additionally, we optimized the quantity of photothermal sensing probes, the laser irradiation power and the duration of irradiation.

The pH environment has an important influence on the coupling efficiency and the dispersibility of the sensing probes. In the process of antibody coupling, if the pH is too low, it can cause coagulation of the material, and if it's too high, it will reduce the coupling efficiency. Therefore, it is very important to find the appropriate coupling pH value. The pH of the solution containing violet phosphorus nanosheets and antibody was adjusted to 6.0 ~ 12.0, and ultraviolet spectrum scanning was performed after coupling (Fig. 3A). When no precipitate was produced after preparation and its OD450 reached the highest value, it was demonstrated that the violet phosphorene nanosheets coupled to the antibody with the highest efficiency and good dispersion. As shown in Fig. S3, the optimal result was obtained at pH = 8.0, which was chosen for the subsequent experiments.

Non-specific binding can affect the detection sensitivity of the immunochromatographic sensor. Therefore, macromolecular substances are frequently selected for blocking buffer to eliminate the influence of non-specific binding. Simultaneously, surfactants are often added to the blocking buffer to enhance the diffusivity, stability and lubricity. Therefore, skim milk powder and Tween-20 were selected as the blocking buffer, and their ratio was optimized. The optimum range for skim milk powder and Tween-20 was 0.5 % ~ 2 %, and the results were shown in Fig. 3B. When the additive amount of skim milk powder and Tween-20 was 1 %, the lightest background color indicated the best blocking capability, and was selected as the most effective component for blocking buffer.

Antibody plays a crucial role in the construction of immunochromatographic sensor. Too low antibody concentration will reduce the sensitivity of the detection, while too high will lead to an increase in cost. In order to achieve a balance between the detection performance and cost, the antibody concentration needs to be optimized. The violet phosphorus nanosheets were incubated with different concentrations of diethylstilbestrol monoclonal antibody (0, 2, 4, 6, 8 and 10 $\mu g \cdot mL^{-1}$). After blocking, the prepared sensing probe was loaded into the immunochromatographic sensor, and the color of the test and control area was observed 10 min later. When the concentration of antibody was 4 $\mu g \cdot mL^{-1}$, the color of the test and control area became clear and no longer significantly improved with higher concentrations. Therefore, 4 $\mu g \cdot mL^{-1}$ was selected as the optimal concentration (Fig. 3C).

Next, the concentrations of antigen and secondary antibody were optimized, respectively. The concentration of the antigen was fixed at 0.5 $mg \cdot mL^{-1}$ and the concentration of the secondary antibody was optimized, ranging from 0.5 to 0.8 $mg \cdot mL^{-1}$. The color reaction in the test and control areas was investigated using negative samples. The group that displayed a uniform and clear color in the control area was determined to have the optimal antigen concentration. As shown in Fig. S4A, the optimal secondary antibody coating concentration in the control area was 0.8 $mg \cdot mL^{-1}$. Then, the concentration of the secondary antibody was fixed at 0.8 $mg \cdot mL^{-1}$ and the concentration of the antigen was optimized within the range of 0.2 to 0.5 $mg \cdot mL^{-1}$. The best antigen concentration in the test area was 0.4 $mg \cdot mL^{-1}$ (Fig. S4B).

Under the optimal conditions mentioned above, the loading amount of the probe based on violet phosphorus nanosheets was optimized from 5 to 25 μL. When the loading amount of the sensing probe was 15 μL, the test and control areas exhibited clear color with clean background.

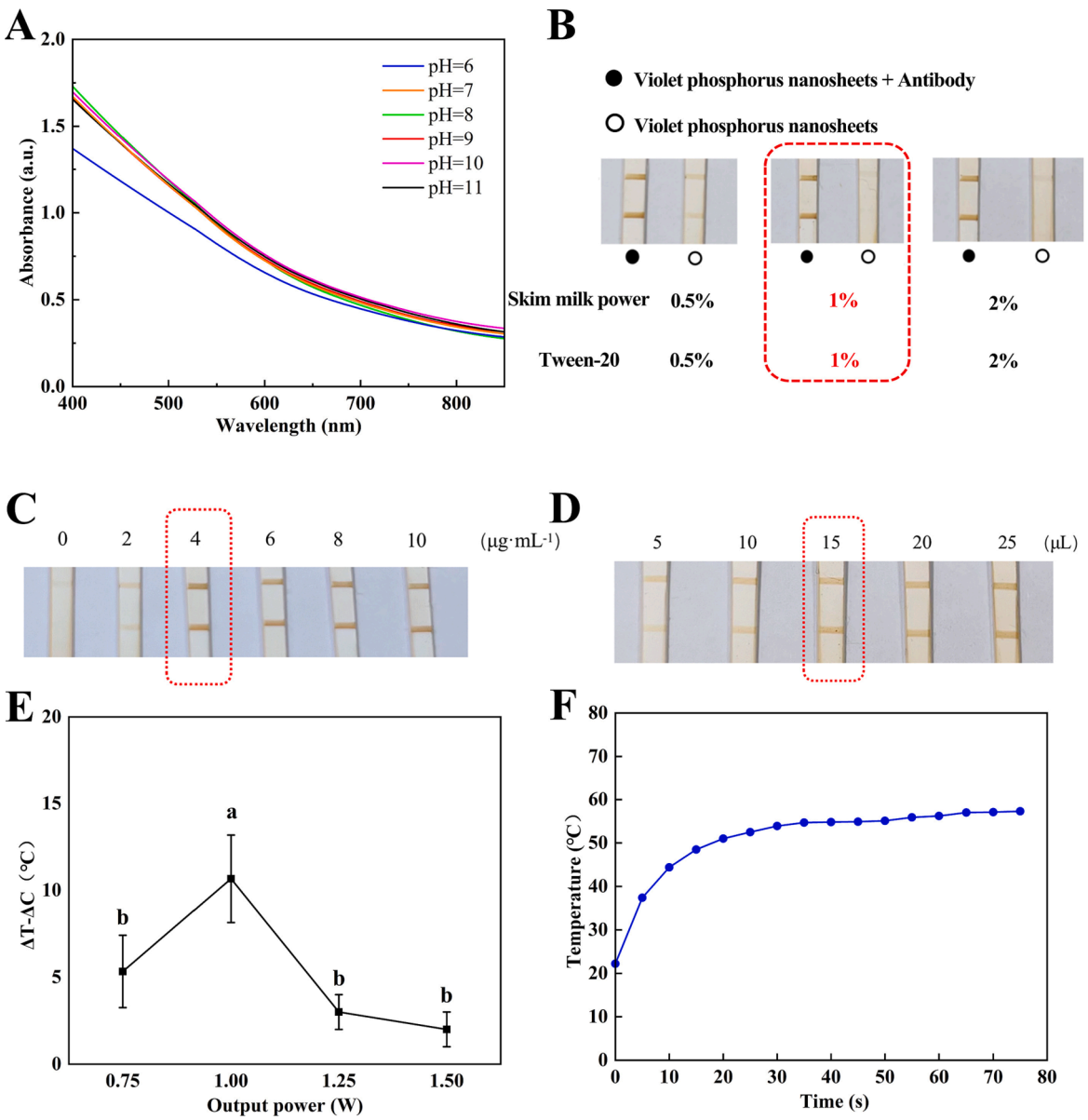


**Fig. 3.** (A) The ultraviolet spectrum of the solution containing violet phosphorus nanosheets and antibody under different pH. Optimization of blocking buffer (B), antibody concentration (C), the loading amount of the probe (D), laser irradiation power (E) and irradiation time (F), different letters represent a significant difference at a level of $p < 0.05$.

Therefore, 15 μL was selected as the optimal loading amount for the final detection process (Fig. 3D).

In addition to optimizing the preparation process of immunochromatographic sensor, it is equally important to enhance the photothermal detection conditions. Previous researches have shown that the laser power and irradiation time have a significant influence on detection results, so the above two conditions were optimized in this study (Lu et al., 2022). The laser irradiation power can directly affect the sensitivity, detection range and signal-to-noise ratio of the detection method, therefore, the laser irradiation power was optimized from 0.75 W to 1.5 W. When the laser power was 1 W, the temperature difference between the detection and control areas was significantly different ($p < 0.05$) with other power, so 1 W was selected as the final power for laser irradiation (Fig. 3E). Then, the irradiation time was optimized, and the results were shown in Fig. 3F. When the irradiation time exceeded 30 s, the temperature of the sensor changed slowly within the dynamic range, so 30 s was chosen as the optimal irradiation time.

### 3.4. Detection range and sensitivity of diethylstilbestrol

The detection principle of the established immunochromatographic sensor is that the antigen in the test area competes with diethylstilbestrol in the sample to bind with the photothermal sensing detection probe. The amount of the probe bound to the test area decreases as the diethylstilbestrol concentration increases. Furthermore, after being irradiated by 808 nm laser, the temperature increase in the test area is also inversely proportional to the diethylstilbestrol concentration. The temperature changes generated by the diethylstilbestrol standard solution on the immunochromatographic sensor were recorded. The standard curve relating diethylstilbestrol concentration to the temperature difference between the test and control areas were obtained, and the quantitative detection of diethylstilbestrol was successfully realized.

The concentrations of diethylstilbestrol standard solution were 0.05, 0.125, 0.25, 0.75, 1.5, 3.0, 6.0, 12.5, 25.0 and 50.0 $\mu g \cdot L^{-1}$, respectively. When the color of the test area was noticeably lighter than that of the control area, the minimum diethylstilbestrol concentration was defined

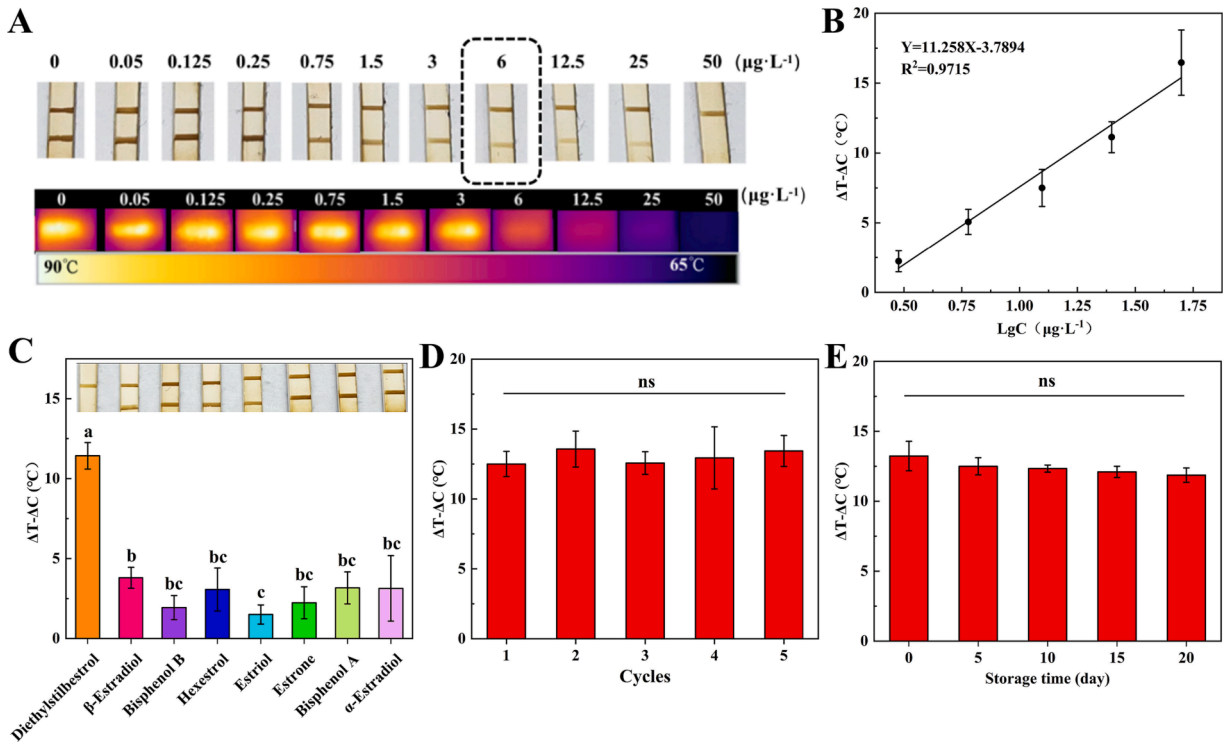


**Fig. 4.** (A) Photographs of visual and photothermal detection of immunochromatographic sensor with diethylstilbestrol standard solution. (B) Standard curve between diethylstilbestrol concentration and temperature difference. Specificity (C), repeatability (D) and stability (E) of immunochromatographic sensor, different letters represent a significant difference at a level of $p < 0.05$, ns means $p > 0.05$ and represents no significance.

as the visual detection limit. As shown in Fig. 4A, the visual detection limit was 6 μg·L$^{-1}$. The standard curve, illustrated in Fig. 4B, displayed a strong linear relationship between diethylstilbestrol concentration and the temperature difference in the range of 0.75 ~ 50 μg·L$^{-1}$. Through calculation, the photothermal detection limit was determined to be 0.56 μg·L$^{-1}$.

Detailed comparisons with previously reported diethylstilbestrol detection methods were shown in Table S2. In comparison with the photothermal sensing method based on gold nanoparticles (20 μg·L$^{-}$1) (Wang, Wang, Wang, Wang, Xu, & Zhang, 2022), the detection limit of our established method (0.56 μg·L$^{-1}$) was significantly improved by 40 times, which further verified raw materials with higher photothermal conversion efficiency can effectively improve the detection sensitivity. The detection limit of the ELISA method was lower, but the detection time was 12 times longer than that of the immunochromatographic sensor (Yang, Wang, Song, Hu, Wang, & Zeng, 2020). Although the detection performance of the microfluidic paper-based analytical chip was slightly better than our method, but its complicated manufacturing process and high cost limited its further application (Wang, Wang, Li, & Zhang, 2023). The detection limit, linear range and detection time of the proposed immunochromatographic sensor were also compared with immunochromatographic assay (Mukunzi, Tochi, Isanga, Liu, Kuang, & Xu, 2016), electrochemical sensor (Pang & Kan, 2020) and colorimetric biosensor (Li, Sun, Salentijn, Ning, Han, Bai, et al., 2022), which were better than the abovementioned diethylstilbestrol detection methods.

### 3.5. The specificity, repeatability and stability of immunochromatographic sensor

In order to evaluate the specificity of the immunochromatographic sensor, β-estradiol, bisphenol B, hexestrol, estriol, estrone, bisphenol A and α-estradiol were selected for non-target determination. The concentration of the sample was 30 μg·L$^{-1}$. All of the samples were incubated with the photothermal sensing probe and then detected by the sensor. The color of the test and control area was observed, and the temperature changes were recorded. As shown in Fig. 4C, when the sample was diethylstilbestrol, the color of the test area was obviously lighter than that of the control area, and the temperature difference between the test and control area exceeded 10 ℃. However, when the detection substance was other estrogens, the color of the test area closely resembled that of the control area. The temperature difference was below 5 ℃ and was significantly lower ($p < 0.05$) than that of diethylstilbestrol samples. The above results demonstrated the significant specificity of the immunochromatographic sensor to diethylstilbestrol.

Five parallel experiments were performed to investigate the repeatability of the immunochromatography sensor, and the results were shown in Fig. 4D and S5. In these parallel tests, there was no statistically significant difference ($p > 0.05$) between the results of visual detection and photothermal detection, demonstrating that the repeatability of the established sensor met the detection requirements.

The storage stability tests of the immunochromatographic sensor were carried out at 4 ℃ over a period of 20 days. During this time, there was a slight degradation in the sensor's detection performance. Twenty days later, there was no statistically significant difference ($p > 0.05$) between the whole detection results. These results indicated that the prepared immunochromatographic sensor had good storage stability (Fig. 4E).

### 3.6. Detection performance in actual samples

To verify the applicability of the proposed immunochromatographic sensor, tap water, milk and pork were selected for addition and recovery experiments. A variety of diethylstilbestrol standard samples with different concentrations (7.5, 15, 30 μg·L$^{-1}$) were added to the actual samples for testing. Due to the complex matrices in the actual samples, including ions in tap water, proteins in milk, and fats in pork products, the detection performance of the established immunochromatographic sensor in these three actual samples differed slightly from that in PBS

**Table 1**
Recovery rates of diethylstilbestrol in actual samples.

| Samples | Spiked concentrations (μg/L) | Immunochromatographic sensor | | | HPLC | | |
|---|---|---|---|---|---|---|---|
| | | Average ± SD (μg/L) | Recovery (%) | CV (%) | Average ± SD (μg/L) | Recovery (%) | CV (%) |
| Tap water | 7.5 | 7.19 ± 0.78 | 95.9 | 10.8 | 7.66 ± 0.80 | 102.1 | 10.4 |
| | 15 | 16.23 ± 1.01 | 108.2 | 6.2 | 14.46 ± 0.33 | 96.4 | 2.3 |
| | 30 | 28.29 ± 2.46 | 94.3 | 8.7 | 27.74 ± 2.13 | 92.5 | 7.7 |
| Milk | 7.5 | 8.14 ± 0.49 | 108.6 | 5.9 | 8.28 ± 1.09 | 110.4 | 13.1 |
| | 15 | 15.57 ± 0.67 | 103.8 | 4.3 | 12.51 ± 1.02 | 83.4 | 8.1 |
| | 30 | 29.77 ± 2.85 | 99.2 | 9.6 | 29.55 ± 2.27 | 98.5 | 7.7 |
| Pork | 7.5 | 7.02 ± 0.73 | 93.6 | 10.4 | 7.19 ± 0.18 | 95.9 | 2.5 |
| | 15 | 16.37 ± 0.33 | 109.1 | 2.0 | 11.94 ± 1.58 | 79.6 | 13.3 |
| | 30 | 31.13 ± 2.28 | 103.8 | 7.3 | 29.32 ± 1.48 | 97.7 | 5.1 |

solution. The recovery rate of diethylstilbestrol in the actual samples ranged from 82.2 % to 115.2 % and the coefficient of variation (CV) was 2.0 %~10.8 % (Table 1 and Fig. S6). These results demonstrated that the constructed novel photothermal sensing probe based on violet phosphorus has good feasibility and applicability in practical diethylstilbestrol immunochromatographic sensing detection.

To further investigate the detection performance of the proposed method, the recovery rate and CV of diethylstilbestrol in the actual samples were compared with HPLC method. As shown in Table 1, The recovery rates of HPLC method in tap water, milk and pork were in the ranged of 92.5 ~ 102.1 %, 83.4 ~ 110.4 %, 79.6 ~ 97.7 %, and the CV was 2.3 ~ 10.4 %, 7.7 ~ 13.1 %, 2.5 ~ 13.3 %, respectively. The above results manifested that the detection performance of the photothermal immunochromatographic sensor based on violet phosphorus was close to HPLC, which further indicated the promising potential of our proposed method for practical applications.

## 4. Conclusion

In summary, the violet phosphorus nanosheets were successfully prepared by ultrasonic spalling method, demonstrating satisfactory stability with a high photothermal conversion rate of 31.1 %. A novel photothermal sensing probe based on violet phosphorus has been developed for the sensitive and quantitative analysis of diethylstilbestrol. The preparation process of the probe and sensing detection conditions were systematically optimized. Under optimal conditions, the visual and photothermal detection limit were 6 $\mu g \cdot L^{-1}$ and 0.56 $\mu g \cdot L^{-1}$, respectively. The diethylstilbestrol concentration showed a good linear relationship with the photothermal signal generated by violet phosphorus based sensing probe within the range of 0.75 ~ 50 $\mu g \cdot L^{-1}$. The immunochromatographic sensor based on violet phosphorus also exhibited excellent specificity, repeatability and stability. The recovery rates of diethylstilbestrol in actual samples of tap water, milk and pork ranged from 82.2 % to 115.2 %, with a coefficient of variation ranging from 2.0 % to 10.8 %. In addition, the potential combination of violet phosphorus with other materials, such as gold nanoparticles, to synthesize new composite materials may hopefully further enhance the photothermal properties of violet phosphorus and improve its photothermal detection performance. This will be a focus of our future work. Our study paves the way for the utilization of violet phosphorus in the field of photothermal detection, opening new avenues for future research and applications.

## CRediT authorship contribution statement

**Zhen Zhang:** Conceptualization, Investigation, Resources, Data curation, Writing – original draft. **Zhenkai Hao:** Methodology, Validation, Formal analysis, Data curation, Visualization. **Ruiping Shan:** Software, Validation, Data curation, Visualization. **Muhammad Wasim Tasleem:** Methodology, Writing – review & editing, Visualization. **Jianbin Wang:** Resources, Methodology. **Jianhua Zhou:** Resources, Writing – review & editing, Methodology. **Hongyan Zhang:** Funding acquisition, Project administration, Supervision, Writing – review & editing, Conceptualization.

## Declaration of competing interest

The authors declare that they have no known competing financial interests or personal relationships that could have appeared to influence the work reported in this paper.

## Data availability

Data will be made available on request.

## Acknowledgments

This work was supported by National Natural Science Foundation of China (Key Program, U22A20550) and the Key Program of the Natural Science Foundation of Shandong Province (ZR2020KC031).

## Appendix A. Supplementary data

Supplementary data to this article can be found online at https://doi.org/10.1016/j.fochx.2023.100990.

## References

Chen, C., Kuo, L., Lee, S., Hwu, Y., Chou, S., Chen, C., … Chen, Y. (2013). Photothermal cancer therapy via femtosecond-laser-excited FePt nanoparticles. *Biomaterials, 34*(4), 1128–1134. https://doi.org/10.1016/j.biomaterials.2012.10.044

Hou, Y., Fei, Y., Liu, Z., Liu, Y., Li, M., & Luo, Z. (2022). Black phosphorous nanomaterials as a new paradigm for postoperative tumor treatment regimens. *Journal of Nanobiotechnology, 20*(1), 366. https://doi.org/10.1186/s12951-022-01579-3

Huang, P., Lin, J., Li, W., Rong, P., Wang, Z., Wang, S., … Chen, X. (2013). Biodegradable gold nanovesicles with an ultrastrong plasmonic coupling effect for photoacoustic imaging and photothermal therapy. *Angewandte Chemie International Edition, 52*(52), 13958–13964. https://doi.org/10.1002/anie.201308986

Ji, Y., Huang, Y., Cheng, Z., Hao, W., Liu, G., Liu, Y., & Zhang, X. (2023). Lateral flow strip biosensors for foodborne pathogenic bacteria via direct and indirect sensing strategies: A review. *Journal of Agricultural and Food Chemistry, 71*(27), 10250–10268. https://doi.org/10.1021/acs.jafc.3c02094

Jin, M., Wang, Y., Gu, M., Zhao, X., Zhao, R., Zhang, Y., … Zhang, J. (2023). Control of crystal growth to obtain needle-shaped violet phosphorus with excellent photocatalytic degradation performance. *Nano Research, 16*(2), 3320–3325. https://doi.org/10.1007/s12274-022-4952-8

Li, G., Li, Q., Wang, X., Liu, X., Zhang, Y., Li, R., … Zhang, G. (2023). Lateral flow immunoassays for antigens, antibodies and haptens detection. *International Journal of Biological Macromolecules, 242*, Article 125186. https://doi.org/10.1016/j.ijbiomac.2023.125186

Li, Q., Sun, T., Salentijn, G. I. J., Ning, B., Han, D., Bai, J., … Wang, Z. (2022). Bifunctional ligand-mediated amplification of polydiacetylene response to biorecognition of diethylstilbestrol for on-site smartphone detection. *Journal of*

*Hazardous materials, 432*, Article 128692. https://doi.org/10.1016/j.jhazmat.2022.128692

Liang, M., Cai, X., Gao, Y., Yan, H., Fu, J., Tang, X., … Li, P. (2022). A versatile nanozyme integrated colorimetric and photothermal lateral flow immunoassay for highly sensitive and reliable Aspergillus flavus detection. *Biosensors and Bioelectronics, 213*, Article 114435. https://doi.org/10.1016/j.bios.2022.114435

Liu, Y., Zhan, L., Qin, Z., Sackrison, J., & Bischof, J. C. (2021). Ultrasensitive and highly specific lateral flow assays for point-of-care diagnosis. *ACS Nano, 15*(3), 3593–3611. https://doi.org/10.1021/acsnano.0c10035

Lu, Z., Liu, W., Cai, Y., Zhao, T., Cui, M., Zhang, H., & Du, S. (2022). Salmonella typhimurium strip based on the photothermal effect and catalytic color overlap of PB@Au nanocomposite. *Food Chemistry, 385*, Article 132649. https://doi.org/10.1016/j.foodchem.2022.132649

Mukunzi, D., Tochi, B. N., Isanga, J., Liu, L., Kuang, H., & Xu, C. (2016). Development of an immunochromatographic assay for hexestrol and diethylstilbestrol residues in milk. *Food and Agricultural Immunology, 27*(6), 855–869. https://doi.org/10.1080/09540105.2016.1183601

Pang, S., & Kan, X. (2020). One-pot synthesis of nitrogen doped graphene-thionine-gold nanoparticles composite for electrochemical sensing of diethylstilbestrol and $H_2O_2$. *Microchemical Journal, 157*, Article 104924. https://doi.org/10.1016/j.microc.2020.104924

Ren, X., Philo, D., Li, Y., Shi, L., Chang, K., & Ye, J. (2020). Recent advances of low-dimensional phosphorus-based nanomaterials for solar-driven photocatalytic reactions. *Coordination Chemistry Reviews, 424*, Article 213516. https://doi.org/10.1016/j.ccr.2020.213516

Salvador, M., Gallo Cordova, Á., Moyano, A., Martínez García, J. C., Blanco López, M. C., Puerto Morales, M., & Rivas, M. (2020). Improved magnetic lateral flow assays with optimized nanotags for point-of-use inductive biosensing. *Analyst, 145*(17), 5905–5914. https://doi.org/10.1039/D0AN00849D

Shang, H., Zhang, X., Ding, M., Zhang, A., & Wang, C. (2023). A smartphone-assisted colorimetric and photothermal probe for glutathione detection based on enhanced oxidase-mimic CoFeCe three-atom nanozyme in food. *Food Chemistry, 423*, Article 136296. https://doi.org/10.1016/j.foodchem.2023.136296

Tu, J., Wu, T., Yu, Q., Li, J., Zheng, S., Qi, K., … Wang, C. (2023). Introduction of multilayered magnetic core–dual shell SERS tags into lateral flow immunoassay: A highly stable and sensitive method for the simultaneous detection of multiple veterinary drugs in complex samples. *Journal of Hazardous materials, 448*, Article 130912. https://doi.org/10.1016/j.jhazmat.2023.130912

Wang, M., Wang, Y., Li, X., & Zhang, H. (2023). Development of a photothermal-sensing microfluidic paper-based analytical chip (PT-Chip) for sensitive quantification of diethylstilbestrol. *Food Chemistry, 402*, Article 134128. https://doi.org/10.1016/j.foodchem.2022.134128

Wang, S., Zhao, X., Liu, Z., Yang, X., Pang, B., Gao, Y., … Kong, M. G. (2023). Violet phosphorus-$Fe_3O_4$ as a novel photocatalysis-self-Fenton system coupled with underwater bubble plasma to efficiently remove norfloxacin in water. *Chemical Engineering Journal, 452*, Article 139481. https://doi.org/10.1016/j.cej.2022.139481

Wang, X., Ma, M., Zhao, X., Jiang, P., Wang, Y., Wang, J., … Zhang, F. (2023). Phase engineering of 2D violet/black phosphorus heterostructure for enhanced photocatalytic hydrogen evolution. *Small Structures.* , Article 2300123. https://doi.org/10.1002/sstr.202300123

Wang, Y., Wang, T., Wang, M., Wang, J., Xu, Z., & Zhang, H. (2022). Photothermal card reader assay using the commercial colloidal gold test strip for the rapid quantitative detection of food hazards. *Microchimica Acta, 189*(3), 112. https://doi.org/10.1007/s00604-022-05193-w

Wang, Z., Wang, M., Wang, X., Hao, Z., Han, S., Wang, T., & Zhang, H. (2023). Photothermal-based nanomaterials and photothermal-sensing: An overview. *Biosensors and Bioelectronics, 220*, Article 114883. https://doi.org/10.1016/j.bios.2022.114883

Wei, M., Rao, H., Niu, Z., Xue, X., Luo, M., Zhang, X., … Lu, X. (2021). Breaking the time and space limitation of point-of-care testing strategies: Photothermometric sensors based on different photothermal agents and materials. *Coordination Chemistry Reviews, 447*, Article 214149. https://doi.org/10.1016/j.ccr.2021.214149

Xia, Y., Hu, X., Liu, Y., Zhao, F., & Zeng, B. (2022). Molecularly imprinted ratiometric electrochemical sensor based on carbon nanotubes/cuprous oxide nanoparticles/titanium carbide MXene composite for diethylstilbestrol detection. *Microchimica Acta, 189*(4), 137. https://doi.org/10.1007/s00604-022-05249-x

Xiao, X., Hu, S., Lai, X., Peng, J., & Lai, W. (2021). Developmental trend of immunoassays for monitoring hazards in food samples: A review. *Trends in Food Science & Technology, 111*, 68–88. https://doi.org/10.1016/j.tifs.2021.02.045

Yang, X., Wang, Y., Song, C., Hu, X., Wang, F., & Zeng, X. (2020). Hapten synthesis and the development of an ultrasensitive indirect competitive ELISA for the determination of diethylstilbestrol in food samples. *Scientific Reports, 10*(1), 3270. https://doi.org/10.1038/s41598-020-59112-1

Younes, N., Yassine, H. M., Kourentzi, K., Tang, P., Litvinov, D., Willson, R. C., … Nasrallah, G. K. (2023). A review of rapid food safety testing: Using lateral flow assay platform to detect foodborne pathogens. *Critical Reviews in Food Science and Nutrition, 1–23*. https://doi.org/10.1080/10408398.2023.2217921

Yuan, H., Chen, P., Wan, C., Li, Y., & Liu, B.-F. (2022). Merging microfluidics with luminescence immunoassays for urgent point-of-care diagnostics of COVID-19. *TRAC Trends in Analytical Chemistry, 157*, Article 116814. https://doi.org/10.1016/j.trac.2022.116814

Zhang, G., Zhang, G., Lai, X., Su, L., He, W., Lai, W., & Deng, S. (2023). Highly sensitive and ultrastable lateral flow immunoassay based on polydopamine-coated aggregation-induced emission fluorescent microspheres with excellent fluorescence performance and biofriendly coupling strategy. *Chemistry of Materials, 35*(9), 3494–3502. https://doi.org/10.1021/acs.chemmater.2c03741

Zhang, L., Gu, M., Li, L., Zhao, X., Fu, C., Liu, T., … Zhang, J. (2020). High yield synthesis of violet phosphorus crystals. *Chemistry of Materials, 32*(17), 7363–7369. https://doi.org/10.1021/acs.chemmater.0c02273

Zhang, L., Huang, H., Zhang, B., Gu, M., Zhao, D., Zhao, X., … Zhang, J. (2020). Structure and properties of violet phosphorus and its phosphorene exfoliation. *Angewandte Chemie International Edition, 59*(3), 1074–1080. https://doi.org/10.1002/anie.201912761

Zhang, S., Huang, Y., Ren, H., Chen, Y., Yan, S., Dai, H., & Lv, L. (2023). Facile and portable multimodal sensing platform driven by photothermal-controlled release system for biomarker detection. *Biosensors and Bioelectronics, 235*, Article 115413. https://doi.org/10.1016/j.bios.2023.115413

Zhang, T., Lei, L., Tian, M., Ren, J., Lu, Z., Liu, Y., & Liu, Y. (2021). Multifunctional $Fe_3O_4$@Au supraparticle as a promising thermal contrast for an ultrasensitive lateral flow immunoassay. *Talanta, 222*, Article 121478. https://doi.org/10.1016/j.talanta.2020.121478

Zhang, Z., Li, S., Qiao, D., Hu, N., Gu, Y., Deng, Q., & Wang, S. (2021). Black phosphorus nanosheet encapsulated by zeolitic imidazole framework-8 for tumor multimodal treatments. *ACS Applied Materials & Interfaces, 13*(37), 43855–43867. https://doi.org/10.1021/acsami.1c04001

Zhao, R., Liu, S., Zhao, X., Gu, M., Zhang, Y., Jin, M., … Zhang, J. (2022). Violet phosphorus quantum dots. *Journal of Materials Chemistry A, 10*(1), 245–250. https://doi.org/10.1039/D1TA09132H

Zhao, Y., Wang, H., Huang, H., Xiao, Q., Xu, Y., Guo, Z., … Chu, P. K. (2016). Surface coordination of black phosphorus for robust air and water stability. *Angewandte Chemie International Edition, 55*(16), 5003–5007. https://doi.org/10.1002/anie.201512038

Zhou, L., Kang, J., Dong, Y., Wang, Y., Li, Y., Huang, H., … He, J. (2023). Solvent-stabilized few-layer violet phosphorus and its ultrafast nonlinear optics. *Nano Research, 16*(4), 5843–5849. https://doi.org/10.1007/s12274-022-5224-3

Zhou, T., Huang, J., Zhao, W., Guo, R., Cui, S., Li, Y., … Zhang, Q. (2022). Multifunctional plasmon-tunable Au nanostars and their applications in highly efficient photothermal inactivation and ultra-sensitive SERS detection. *Nanomaterials, 12*(23), 4232. https://doi.org/10.3390/nano12234232